analytical chemistry

pubs.acs.org/ac Article

Effective Chiral Discrimination of Amino Acids through Oligosaccharide Incorporation by Trapped Ion Mobility Spectrometry

Chengyi Xie, Liancheng Gu, Qidi Wu, Lei Li, Chenlu Wang, Jiancheng Yu,* and Keqi Tang*

Cite This: *Anal. Chem.* 2021, 93, 859−867 Read Online

ACCESS | Metrics & More | Article Recommendations | Supporting Information

ABSTRACT: Chiral analysis is critical to many research fields due to different biological functions of enantiomers in living systems. Although the use of ion mobility spectrometry (IMS) has become an alternative technology in the area of chiral measurements, there is still a lack of a general chiral selector for IMS-based chiral recognition, especially for small chiral molecules. Here, a new method using oligosaccharides as the chiral selector has been developed to discriminate chiral amino acids (AAs) by trapped ion mobility spectrometry-mass spectrometry (TIMS-MS). We analyzed 21 chiral amino acids, including small molecules (e.g., alanine and cysteine). Our data showed that the use of nonreducing tetrasaccharides was effective for the separation of chiral AAs, which differentiated 21 chiral AAs without using metal ions. By further incorporating a copper ion, the separation resolution could be improved to 1.64 on average, which accounts for an additional 52% improvement on top of the already achieved separation in metal-free analysis. These results indicate that the use of tetrasaccharides is an effective strategy for the separation of AA enantiomers by TIMS. The method developed in this study may open up a new strategy for effective IMS-based chiral analysis.

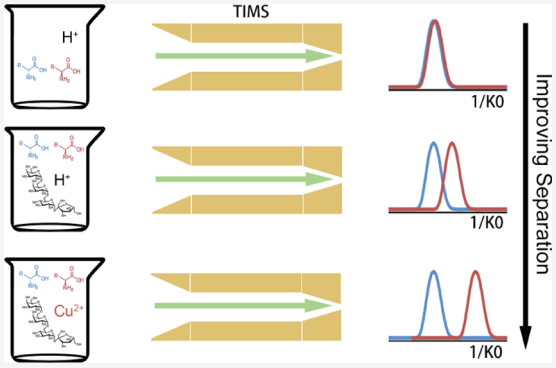

INTRODUCTION

Recently, considerable attention has been paid to chiral compound analysis because of the critical roles of chirality in biological and pharmaceutical science. Most biology-related compounds, such as amino acids, carbohydrates, and nucleic acids, are chiral. The chiral environment of living systems possibly makes the biological behavior of enantiomers dramatically different.[1,2] However, the identical physical and chemical properties of enantiomers have made chiral identification one of the most challenging tasks in biological analysis.

Several chromatographic techniques, including gas chromatography (GC),[3] liquid chromatography (LC),[4] and supercritical fluid chromatography (SFC),[5] have been widely used in chiral analysis. In general, chiral stationary phases are involved in these methods. Capillary electrophoresis (CE) has also been well developed for chiral analysis.[6] However, both chromatography- and electrophoresis-based methods require at least dozens of minutes to accomplish separation.

The introduction of mass spectrometry (MS) could provide fast and sensitive analysis for a specific analyte, which well overcomes the analytical limitations of chromatography- or electrophoresis-based methods. Despite these considerable advantages, enantiomers cannot be distinguished directly by MS due to the same molecular weight. In an effort to unlock this critical bottleneck, enantiomers are generally transformed into diastereomeric complexes using chiral agents and then distinguished based on (i) the intensity difference of diastereomers,[7,8] (ii) the kinetic methods with tandem MS technologies,[9−13] or (iii) the measurements of the rates of the gas-phase ion−molecule reactions.[14−16] However, all of these MS-based methods are indirect, and the interpretation of mass spectra in a chiral mixture is relatively complex.

Recently, ion mobility spectrometry (IMS) has become a promising alternative technology in the area of isomeric differentiation.[17] As a postionization separation method in the gas phase, IMS provides the separation of ions based on their average collision cross section (CCS), which mainly depends on their size, shape, and charge state. Different IMS technologies, including linear[18−21] or nonlinear[22] methods, have been used for chiral analysis.[23] In 2006, Dwivedi et al.[24] demonstrated the separation of enantiomers by creating a chiral environment in the IMS drift tube. Some chiral pharmaceuticals, amino acids, and carbohydrates were resolved by doping the drift gas with 2-butanol in drift tube IMS. Other

Received: August 13, 2020
Accepted: November 10, 2020
Published: November 23, 2020

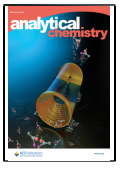

https://dx.doi.org/10.1021/acs.analchem.0c03461
Anal. Chem. 2021, 93, 859−867

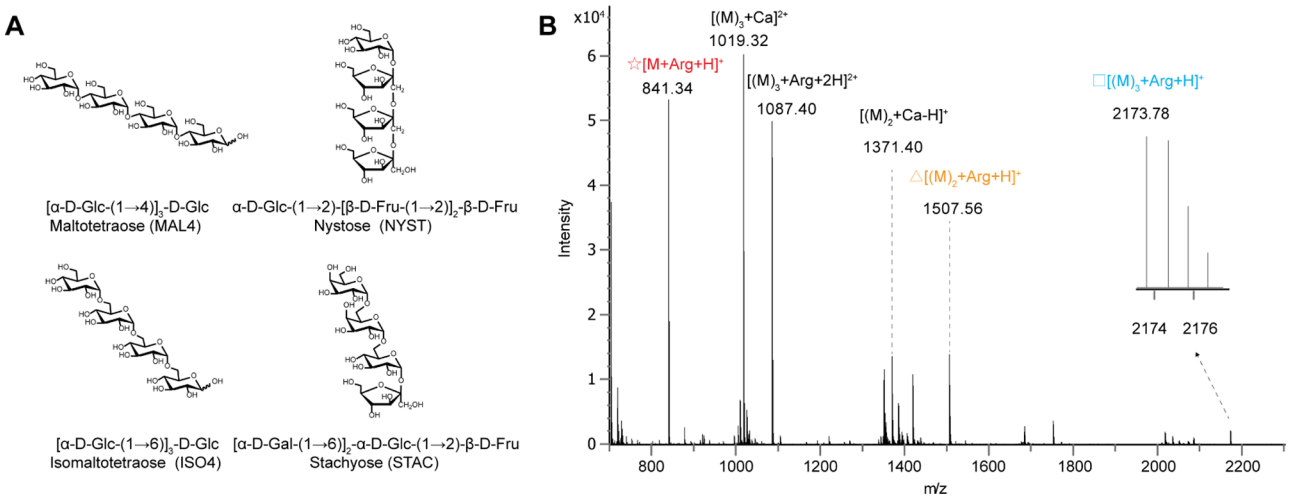

Figure 1. (A) Structures of the four tetrasaccharides used in this study and (B) mass spectrum obtained from an NYST and Arg mixture.

method development efforts have concentrated on increasing the CCS difference of enantiomers by pretreatment strategies, including the formation of noncovalent complexes during electrospray ionization (ESI)[25−29] or derivatization methods.[30] Normally, metal ion-bound trimeric or tetrameric complexes, which are of analyte amino acids, reference amino acids, and metal ions, were chosen for chiral recognition.[25,26] To date, there has been still a lack of effective IMS-based methods for chiral discrimination of small molecules, such as alanine (Ala) and cysteine (Cys). Therefore, finding a general chiral agent is exceptionally crucial for in-depth application of IMS-based chiral analysis.

In this work, we proposed a new IMS-based approach using oligosaccharides as the chiral selector to differentiate enantiomers. Protonated complex ions $[(M)_n + AA + H]^+$ (where M is a tetrasaccharide and AA is an amino acid) were chosen and analyzed using trapped ion mobility spectrometry (TIMS). To begin with, we investigated four tetrasaccharides and found that nonreducing tetrasaccharides were more suitable for chiral AA separation. In comparison with negative ion mode, positive ion mode could provide better resolving ability for the tetrasaccharide−AA complex ion. This form of complex ion was further used to evaluate the separation of 21 chiral AAs, including small molecules. Moreover, we also investigated the influence of the combination of both a copper ion and tetrasaccharides on the separation of chiral AAs, due to the wide use of copper ions in chiral analysis.[9,10,13,25−27]

EXPERIMENTAL SECTION

Chemicals. D- and L-Arginine (Arg), histidine (His), aspartic acid (Asp), glutamic acid (Glu), threonine (Thr), asparagine (Asn), glutamine (Gln), cysteine·(Cys)·HCl·H_2O, alanine (Ala), valine (Val), isoleucine (Ile), leucine (Leu), methionine (Met), tyrosine (Tyr), tryptophan (Trp), ornithine (Orn)·HCl, aminoadipic acid (Aad), pipecolic acid (Pipe), D-serine (D-Ser), D-proline (D-Pro), and $CuCl_2$ were purchased from Aladdin Co., Ltd. (Shanghai, China). D- and L-Phenylalanine (Phe), L-serine (L-Ser), and L-proline (L-Pro) were purchased from Sinopharm Chemical Reagent Co., Ltd. (Shanghai, China). Maltotetraose (MAL4) was purchased from Solarbio Science and Technology Co. Ltd. (Beijing, China). Isomaltotetraose (ISO4) was purchased from TCI Development Co., Ltd. (Shanghai, China). Stachyose (STAC)·$4H_2O$ and nystose (NYST) were purchased from Shanghai Yuanye Biological Technology Co., Ltd. (Shanghai, China). Formic acid and methanol were purchased from Fisher Scientific Inc. (Pittsburgh, PA). An ESI-L Low Concentration Tuning Mix was purchased from Agilent Technologies (Santa Clara, CA).

Sample Preparation. Amino acids, tetrasaccharides, and $CuCl_2$ stock solutions were individually prepared using deionized water from a Milli-Q water purification system (Bedford, MA) to achieve a concentration of 500 μM. For metal-free analysis, a tetrasaccharide solution was first mixed with an amino acid solution at a 1:1 vol ratio and then diluted with a MeOH/water/formic acid solution (50:50:0.1, v/v/v) to a concentration of 20 μM each in the sample mixture. For the copper ion binding studies, $CuCl_2$, tetrasaccharide, and amino acid solutions were mixed with equal volume ratio and diluted with a MeOH/water solution (1:1, v/v) to a final concentration of 20 μM each in the sample mixture. The concentration of analyte was optimized according to the observed intensity of the complex ion, and better complex formation was observed for higher analyte concentration. Additionally, the 50 μM amino acid solution was prepared by diluting the 500 μM amino acid solution with a MeOH/water/formic acid solution (50:50:0.1, v/v/v) for direct AA analysis.

Trapped Ion Mobility Spectrometry. All chiral analysis experiments were performed on a Bruker timsTOF instrument (Bremen, Germany), equipped with an electrospray ionization (ESI) source operated in both positive and negative modes. For positive mode analysis, end plate offset and capillary voltages were set at 500 and 4500 V, respectively. A nebulizer was set at 0.4 bar, and dry gas was heated to 200 °C at a flow rate of 4 L/min. In the negative mode, other ion source parameters remained the same as in the positive mode, but capillary voltage was set at 3200 V. A syringe pump was used for direct injection of samples with a glass syringe of 500 μL from Hamilton (Giarmata, Romania) at a flow rate of 3 μL/min. For the TIMS analyzer, both the $1/K_0$ (K_0 is reduced mobility) range and ramp time were optimized to achieve the maximum resolving power for a specific analyte ion. Specifically, the ramp time was set to a maximum (518 ms in most cases). The $1/K_0$ range was adjusted depending on the $1/K_0$ value of the specific ion. In practice, the TIMS analysis was first performed in a wide $1/K_0$ range (0.6−2.1 V·s/cm^2) to

https://dx.doi.org/10.1021/acs.analchem.0c03461
Anal. Chem. 2021, 93, 859−867

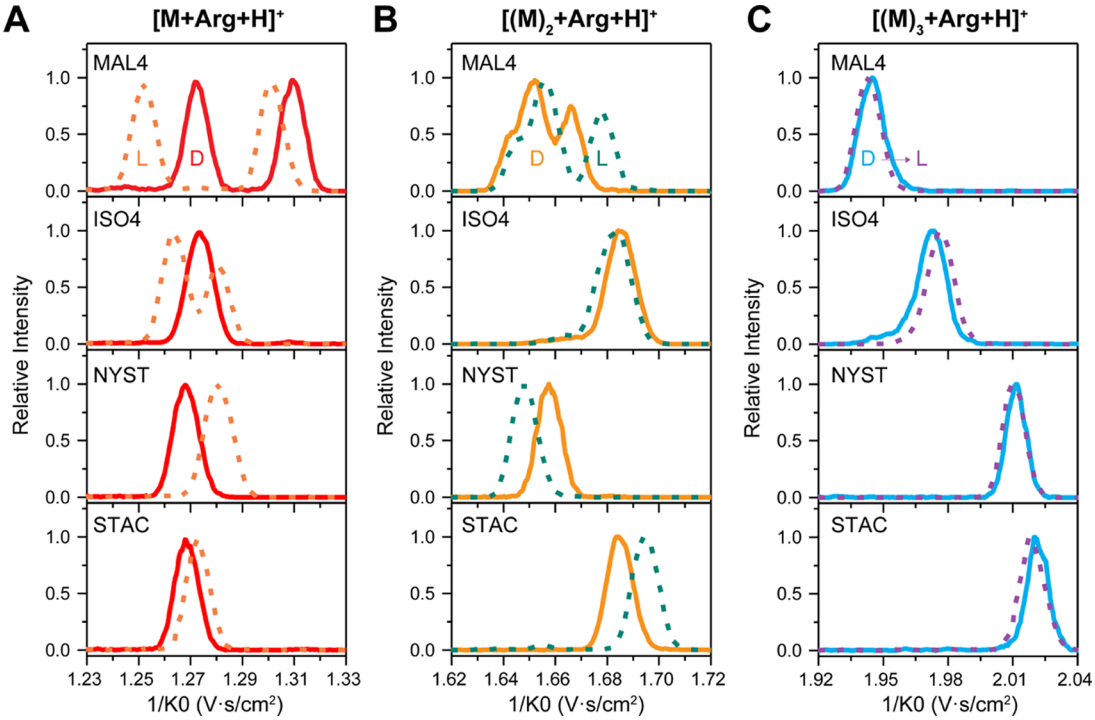

Figure 2. $1/K_0$ distributions of tetrasaccharide and Arg complexes (solid lines for D-form and dashed lines for L-form), including (A) dimeric ions $[M + Arg + H]^+$, (B) trimeric ions $[(M)_2 + Arg + H]^+$, and (C) tetrameric ions $[(M)_3 + Arg + H]^+$.

obtain the $1/K_0$ value of the analyte ion. A smaller $1/K_0$ range was then set according to the obtained $1/K_0$ value, but this range also included the $1/K_0$ values of two or three ions in the Agilent tuning mix to allow accurate TIMS measurement calibration. The detailed parameters of the ramp time and $1/K_0$ range are reported in the Results and Discussion section. The accumulation time was 50 ms to ensure adequate signal intensity of analyte ions. Mass and ion mobility calibration was performed at the beginning of each experiment using the Agilent ESI-L Low Concentration Tuning Mix.

Data Analysis. The resolving power (R) and resolution (r) of the measured mobilograms are defined as $R = A/W_{FWHM}$ and $r = 2.35 \times (A_2 - A_1)/(2 \times W_{FWHM1} + 2 \times W_{FWHM2})$, where A is the $1/K_0$ value of the analyte ion and W_{FWHM} is the full peak width at half-maximum (FWHM). All resolving power, FWHM, and $1/K_0$ values were obtained using Bruker Compass DataAnalysis 5.1.

RESULTS AND DISCUSSION

Selection of Oligosaccharides for Chiral AA Analysis. Four different tetrasaccharides (Figure 1A), including two reducing oligosaccharides (maltotetraose and isomaltotetraose) and two nonreducing oligosaccharides (nystose and stachyose), were used in the initial experimental investigation to find a suitable chiral reference with good resolution for different chiral amino acids (AAs) because we found that the tetrasaccharide could form noncovalent complexes with AA, which enable mobility difference for chiral AAs. Chiral Arg was chosen as a model sample to study the complex patterns of tetrasaccharides and AAs under ESI. A wide $1/K_0$ range (0.6–2.1 V·s/cm^2) was set at first to provide sufficient ion mobility range for all possible complex ions of tetrasaccharides and AAs. A typical mass spectrum obtained from the NYST and D-Arg solution is presented in Figure 1B. For noncovalent bonding products of NYST and D-Arg, protonated multimeric complexes $[NYST + D\text{-}Arg + H]^+$, $[(NYST)_2 + D\text{-}Arg + H]^+$, and $[(NYST)_3 + D\text{-}Arg + H]^+$ were observed and verified through their monoisotopic masses. The same multimeric forms are also found in the ESI mass spectra of other tetrasaccharide and AA solutions in Figure S1. For observed calcium adducts, calcium ions presumably came from the glass container used during sample preparation, and they easily bonded with NYST.

The ion $1/K_0$ distributions of Arg and tetrasaccharide complexes for MAL4, ISO4, NYST, and STAC are shown in Figure 2. For dimeric complexes in Figure 2A, both ions $[MAL4 + D\text{-}Arg + H]^+$ and $[MAL4 + L\text{-}Arg + H]^+$ presented two analyte peaks in the TIMS spectra, which may be caused by different anomeric configurations (α- and β-anomers) of MAL4. This result is similar to the presence of multiple analyte peaks in the IMS analysis of sodiated oligosaccharides.[31] The formation of these peaks was investigated by a cyclic ion mobility (cIM) instrument and largely resulted from the coexisting anomeric forms of oligosaccharides.[32] This inference could also be confirmed by the presence of two analyte peaks of the reducing oligosaccharide complex $[ISO4 + L\text{-}Arg + H]^+$, while a single peak was observed for nonreducing oligosaccharide complexes $[STAC + Arg + H]^+$ and $[NYST + Arg + H]^+$. However, only the single IMS peak was preserved for the D-Arg complex $[ISO4 + D\text{-}Arg + H]^+$ (Figure 2A), even though ISO4 has a reducing-end moiety, possibly due to the subtle mobility difference between the α-anomer and β-anomer of the complex $[ISO4 + D\text{-}Arg + H]^+$, which could not be distinguished under the current TIMS resolution. When it comes to trimeric ions, the $1/K_0$ difference between the two conformers decreased from 0.0372 V·s/cm^2 for the complex $[MAL4 + D\text{-}Arg + H]^+$ (Figure 2A) to 0.0141 V·s/cm^2 for the complex $[(MAL4)_2 + D\text{-}Arg + H]^+$ (Figure 2B). These two conformers finally merged into a single peak for the complex $[(MAL4)_3 + D\text{-}Arg + H]^+$ (Figure 2C). The same trend also

https://dx.doi.org/10.1021/acs.analchem.0c03461
Anal. Chem. 2021, 93, 859−867

holds for the MAL4−L-Arg complexes in Figure 2. Similarly, the two analyte peaks of the complex [ISO4 + L-Arg + H]$^+$ also turned out to be a single peak for the complex [$(ISO4)_2$ + L-Arg + H]$^+$ (Figure 2B).

By incorporating different oligosaccharides, varying IMS 1/K_0 differences could be observed between the D- and L-Arg complexes. Interestingly, the front eluting conformers of the complex [MAL4 + Arg + H]$^+$ could achieve a larger 1/K_0 difference (0.0205 V·s/cm^2) between D and L when compared to the conformers at the back (0.0083 V·s/cm^2) with higher 1/K_0 values in Figure 2A. For ISO4 complexes, the 1/K_0 of the complex [ISO4 + D-Arg + H]$^+$ was between the two 1/K_0 values corresponding to two [ISO4 + L-Arg + H]$^+$ complexes. Hence, the peak of the ISO4-D-Arg complex is largely unresolved from any peak of the ISO4−L-Arg complex in the sample mixture. For nonreducing oligosaccharide complexes, ions [NYST + D/L-Arg + H]$^+$ showed a larger 1/K_0 difference (0.0124 V·s/cm^2) between D and L as compared to 0.0049 V·s/cm^2 for ions [STAC + D/L-Arg + H]$^+$. Considering trimeric ions in Figure 2B, the 1/K_0 difference between D and L for ions [$(MAL4)_2$ + D/L-Arg + H]$^+$, [$(ISO4)_2$ + D/L-Arg + H]$^+$, and [$(NYST)_2$ + D/L-Arg + H]$^+$ decreased when compared to their corresponding dimeric ions [M + D/L-Arg + H]$^+$ in Figure 2A. By contrast, the 1/K_0 difference between ions [$(STAC)_2$ + D-Arg + H]$^+$ and [$(STAC)_2$ + L-Arg + H]$^+$ increased in comparison with the dimeric ions [STAC + Arg + H]$^+$ in Figure 2A. For tetrameric ions in Figure 2C, there is no obvious 1/K_0 difference observed between D-Arg and L-Arg for all four tri−tetrasaccharide complexes.

In addition to the changed 1/K_0 difference, different elution orders of the chiral Arg could be achieved by incorporating different oligosaccharides. For example, the complex [MAL4 + D-Arg + H]$^+$ presents higher 1/K_0 (lower mobility) than the corresponding L-Arg complex in Figure 2A. This suggests that a more extended structure was exhibited for the MAL4−D-Arg complex than the MAL4−Arg complex in the gas phase. In contrast, Arg complexes showed reversed 1/K_0 distributions for D and L by incorporating NYST, and the elution order of D- and L-Arg was reversed again for the di-NYST−Arg complexes in Figure 2B. These experimental observations reveal the great influence of oligosaccharides on the IMS distributions of chiral amino acids.

The analysis above strongly demonstrates the great potential of oligosaccharides used as the reference compound to distinguish chiral amino acids. Additionally, the 1/K_0 difference between D- and L-Arg complexes varies greatly with the selection of different types of tetrasaccharides (MAL4, ISO4, STAC, and NYST) or different multimeric forms ([M + Arg + H]$^+$, [$(M)_2$ + Arg + H]$^+$, and [$(M)_3$ + Arg + H]$^+$). Although reducing oligosaccharides may achieve higher 1/K_0 difference sometimes, the multiple analyte peaks may lead to the misunderstanding and complexity of chiral analysis. Therefore, our further experiments will mainly concentrate on the nonreducing oligosaccharides (NYST and STAC) and their multimeric complexes on chiral amino acid differentiation by TIMS.

Effects of Tetrasaccharides for AA Separation. For the purpose of further substantiating the effect of nonreducing tetrasaccharides (NYST and STAC) on the separation of chiral amino acid mixtures, the TIMS separation of the mixtures of D- and L-Arg or D- and L-Trp is shown in Figure 3. The complexes [NYST + Arg + H]$^+$ and [$(STAC)_3$ + Trp + H]$^+$ showed a larger 1/K_0 difference than other complexes from the TIMS

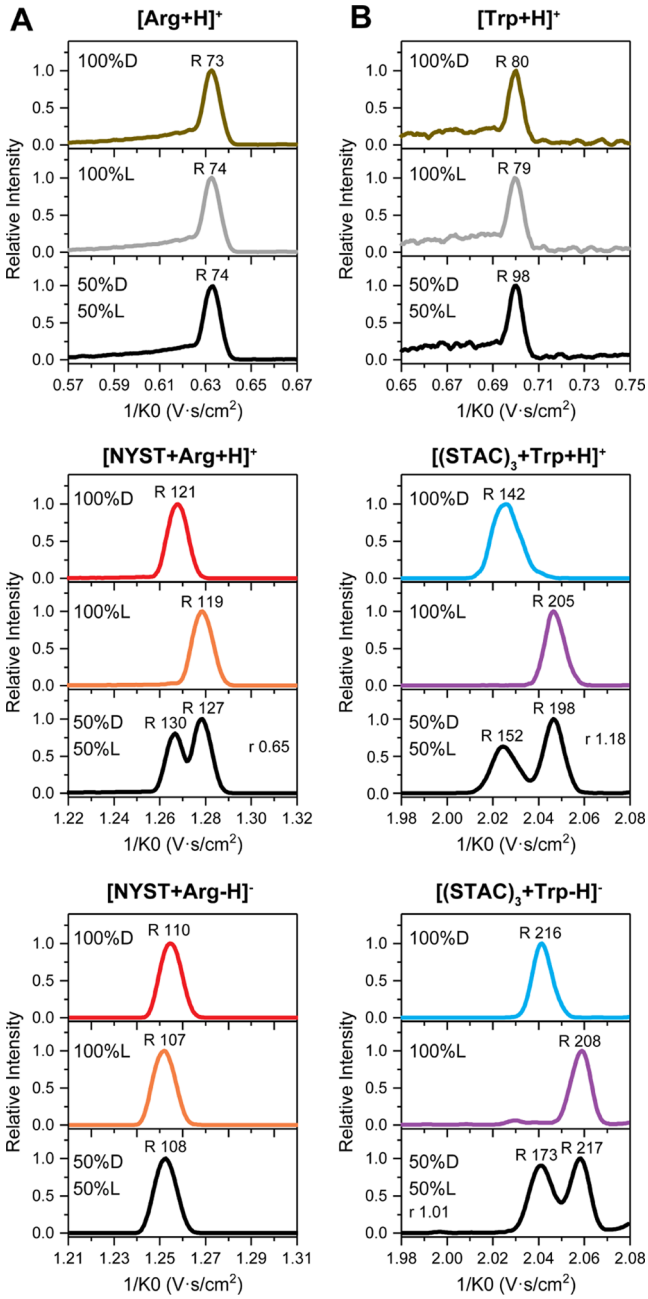

Figure 3. TIMS separation for protonated AAs and tetrasaccharide−AA complexes, including (A) Arg and (B) Trp. The 1/K_0 distributions of the individual samples and sample mixtures are depicted in colored and black traces, respectively. The *R* and *r* values are also given.

analysis in a wide mobility range and therefore were chosen for chiral separation by TIMS. For comparison purposes, the protonated Arg and Trp analysis is presented in the first panel of Figure 3. In an effort to find the optimum ion polarity for chiral AA separation, both positive and negative ions of oligosaccharide and AA complexes were explored as well. The TIMS distributions of pure standard samples were presented along with the mixture analysis to exclude other possibilities (e.g., multiple protonation sites) that may lead to multiple peaks. To achieve the optimum separation, the 1/K_0 range of TIMS setting was optimized according to the 1/K_0 value obtained in the wide 1/K_0 range TIMS measurement.

https://dx.doi.org/10.1021/acs.analchem.0c03461
Anal. Chem. 2021, 93, 859−867

Table 1. Values of the m/z, $1/K_0$ Range, Elution Order, $1/K_0$ Difference, Resolving Power, and Resolution for STAC−AA Complexes Obtained by TIMS Analysis

AA	observed ion	observed m/z	$1/K_0$ range (V·s/cm^2)	front elution enantiomer	$1/K_0$ difference (V·s/cm^2)	R_D	R_L	r
Phe	$[(STAC)_2 + Phe + H]^+$	1498.53	1.53−1.75	L	0.0090	191	197	0.60
Gln	$[(STAC)_3 + Gln + H]^+$	2145.74	1.86−2.05	D	0.0122	192	182	0.67
Ala	$[STAC + Ala + H]^+$	756.28	1.17−1.41	D	0.0096	129	132	0.61
Arg	$[(STAC)_2 + Arg + H]^+$	1507.56	1.53−1.75	D	0.0109	196	191	0.74
His	$[STAC + His + H]^+$	822.30	1.17−1.41	L	0.0112	151	152	0.79
Thr	$[(STAC)_2 + Thr + H]^+$	1452.51	1.53−1.75	L	0.0127	189	190	0.84
Ile	$[STAC + Ile + H]^+$	798.32	1.17−1.41	D	0.0171	127	132	1.04
Val	$[STAC + Val + H]^+$	784.31	1.17−1.41	D	0.0187	133	134	1.20
Pro	$[(STAC)_2 + Pro + H]^+$	1448.51	1.53−1.75	L	0.0122	210	215	0.91
Ser	$[(STAC)_2 + Ser + H]^+$	1438.49	1.53−1.75	L	0.0084	176	212	0.57
Glu	$[(STAC)_3 + Glu + H]^+$	2146.72	1.86−2.05	D	0.0251	203	138	1.21
Leu	$[STAC + Leu + H]^+$	798.32	1.17−1.41	D	0.0092	129	119	0.53
Trp	$[(STAC)_3 + Trp + H]^+$	2203.76	1.86−2.05	D	0.0212	189	218	1.24
Met	$[(STAC)_3 + Met + H]^+$	2148.72	1.86−2.05	L	0.0099	202	212	0.60
Asn	$[(STAC)_2 + Asn + H]^+$	1465.50	1.53−1.75	L	0.0280	181	189	1.80
Cys	$[(STAC)_2 + Cys + H]^+$	1454.47	1.53−1.75	L	0.0078	179	224	0.55
Orn	$[(STAC)_2 + Orn + H]^+$	1465.54	1.53−1.75	L	0.0135	198	198	0.94
Pipe	$[(STAC)_2 + Pipe + H]^+$	1462.53	1.53−1.75	L	0.0187	219	214	1.41
Asp	$[STAC + Asp + H]^+$	800.27	1.17−1.41	D	0.0289	108	109	1.52
Aad	$[(STAC)_2 + Aad + H]^+$	1494.52	1.53−1.75	L	0.0146	198	191	0.98
Tyr[a]	$[(STAC)_2 + Tyr + H]^+$	1514.52	1.53−1.75	L	0.0056	166	168	0.32

[a]Undistinguished chiral mixture; the $1/K_0$, R, and r values obtained in individual analysis.

Although the $1/K_0$ range may shift to higher or lower values for different complex ions, the $1/K_0$ difference (0.4 V·s/cm^2) and ramp time (370 ms) were kept constant to make the TIMS separation data comparable. Specifically, the $1/K_0$ range was set at 0.40−0.80 V·s/cm^2 for ions $[Arg + H]^+$ and $[Trp + H]^+$, 1.17−1.57 V·s/cm^2 for ions $[NYST + Arg + H]^+$, 1.21−1.61 V·s/cm^2 for ions $[NYST + Arg - H]^-$, and 1.68−2.08 V·s/cm^2 for ions $[(STAC)_3 + Trp + H]^+$ and $[(STAC)_3 + Trp - H]^-$ in TIMS analysis. As shown in the first panel of Figure 3A, the TIMS distributions of the protonated AAs $[D\text{-}Arg + H]^+$ (0.6325 V·s/cm^2) and $[L\text{-}Arg + H]^+$ (0.6325 V·s/cm^2) were exactly identical. Not surprisingly, no signs of separation were observed for the D and L mixture ions $[DL\text{-}Arg + H]^+$. This result is consistent with the result of a previous study that chiral amino acids could not be distinguished by IMS directly.[25] By incorporating NYST, considerable $1/K_0$ difference between ions $[NYST + D\text{-}Arg + H]^+$ and $[NYST + L\text{-}Arg + H]^+$ of about 0.0108 V·s/cm^2 was obtained in individual sample analysis. Under the same experimental condition, ions $[NYST + D\text{-}Arg + H]^+$ and $[NYST + L\text{-}Arg + H]^+$ could achieve half-valley resolution in the sample mixture with $r \sim 0.65$, whose mobility distributions were consistent with the individual sample analysis. Therefore, the chiral Arg was indeed resolved through incorporating di-STAC. In contrast, the $1/K_0$ difference of about 0.0028 V·s/cm^2 between ions $[NYST + D\text{-}Arg - H]^-$ and $[NYST + L\text{-}Arg - H]^-$ obtained in negative mode was not large enough to distinguish chiral Arg in the sample mixture. For protonated Trp, there was basically no $1/K_0$ difference observed between ions $[D\text{-}Trp + H]^+$ and $[L\text{-}Trp + H]^+$, and therefore, no separation was achieved for the mixture ions $[DL\text{-}Trp + H]^+$ in the TIMS dimension. By choosing the STAC complexes, the $1/K_0$ difference between ions $[(STAC)_3 + D\text{-}Trp + H]^+$ and $[(STAC)_3 + L\text{-}Trp + H]^+$ was strikingly large to achieve nearly baseline separation with $r \sim 1.18$, while the negative charge state only provided half-valley resolution for ions in the sample mixture. Other amino acids were further investigated by TIMS, but only four of them (Phe, His, Tyr, and Aad) with a relatively large molecular weight were observed in the protonated form. The analysis above for the chiral Arg and Trp was also preserved for all of these four AAs. The detailed experimental data similar to Figure 3 is presented in Figure S2. Additionally, higher resolving power was observed for the tetrameric ions ($R > 150$) as compared to the dimeric ions ($R \sim 100$) and monomeric ions ($R < 100$) in both positive and negative ion modes (Figure 3) because ions with larger $1/K_0$ values (lower mobility) generally achieve higher resolving power in TIMS.[33] In conclusion, all experimental data fully demonstrate that chiral AAs could not be discriminated by TIMS directly because nearly the same $1/K_0$ values were presented for the protonated D and L forms. The incorporation of oligosaccharides was very effective for the TIMS separation of chiral amino acids. More importantly, the positive ions normally provide a better separation than the negative ions for the oligosaccharide and AA complexes.

To get general trends of the effect of nonreducing tetrasaccharides on chiral amino acid IMS separation, we further conducted TIMS analysis of all nonreducing tetrasaccharide (NYST and STAC) and AA (21 pairs used in our experiments) complexes. These samples were analyzed in the wide $1/K_0$ range (0.6−2.1 V·s/cm^2) to obtain all multimeric ions (dimers, trimers, and tetramers) mentioned above. The two-dimensional (2D) scatter plots of $1/K_0$ vs m/z for all amino acid and tetrasaccharide complexes are presented in Figure S3. Based on the $1/K_0$ difference gathered in the wide $1/K_0$ range, the STAC (NYST) complexes with the largest $1/K_0$ difference for each AA were chosen to investigate the separation for each chiral mixture used in this study. Similar to the TIMS setting in Figure 3, the $1/K_0$ range was optimized for each analyte sample. The values of the m/z, $1/K_0$ range, elution order, $1/K_0$ difference, R, and r obtained from these complexes are shown in Tables 1 and S1. For unresolved chiral

https://dx.doi.org/10.1021/acs.analchem.0c03461
Anal. Chem. 2021, 93, 859−867

AA complexes in the sample mixture, the $1/K_0$ difference, R, and r values were obtained in individual AA analysis. Among all separated pairs of complexes in Tables 1 and S1, the $1/K_0$ difference of 0.0078 V·s/cm^2 between ions $[(STAC)_2$ + D-Cys + H$]^+$ and $[(STAC)_2$ + L-Cys + H$]^+$ was large enough to be distinguished by TIMS under $R \sim 200$. Strikingly, for all 21 chiral amino acids used in this study, 20 of them were resolved using STAC complexes in Table 1. To our knowledge, the use of STAC as the chiral reference could achieve the maximum number of chiral amino acid separation when compared to other specific compound references[25−29] or derivatization methods[30] in IMS analysis. Moreover, our method has the simplest sample pretreatment process, which could be accomplished by simply mixing stachyose and amino acid solutions with an equal volume ratio. Only chiral Tyr could not be resolved using the STAC complexes, which displayed one feature (1.7148 V·s/cm^2) in the [STAC + DL-Tyr + H$]^+$ mixture. Specifically, the resolving power of ∼168 is insufficient to distinguish the sample mixture of ions [STAC + D-Tyr + H$]^+$ and [STAC + L-Tyr + H$]^+$ under the $1/K_0$ difference of ∼0.0056 V·s/cm^2 measured in individual analysis. However, the chiral Tyr could be easily separated by choosing the NYST complexes [NYST + Tyr + H$]^+$ under R of slightly more than 100 and r of ∼0.84 in Table S1. Similarly, the chiral Asn, Cys, and Pipe, which could not be discriminated using NYST complexes, could be resolved by STAC complexes with $r \sim 1.8$, 0.55, and 1.41, respectively. Comparison of STAC with NYST on chiral separation shows that STAC is a better choice if we consider performing chiral analysis with only one tetrasaccharide by TIMS because using STAC complexes could resolve almost all AAs used in our experiments.

By comparing the resolution values obtained in Tables 1 and S1, the optimum separation for each chiral AA is presented in Figure 4 under the same TIMS setting conditions. Nearly baseline or baseline separation could be achieved through incorporating tetrasaccharide (STAC or NYST) for most chiral AAs studied. Most importantly, the chiral Cys, Ala, and Asp, which have not been discriminated so far by any other IMS methods,[24−30] could be separated in this study (Figure 4). However, only slightly resolved peaks were achieved for chiral Cys ($r \sim 0.55$) and Phe ($r \sim 0.6$). We speculate that the separation of these chiral AAs could be improved using nonreducing oligosaccharides other than STAC and NYST based on the above experimental findings. The $1/K_0$ difference ranges from 0.0078 V·s/cm^2 for Cys to 0.0289 V·s/cm^2 for Asp and the r values range from 0.55 for Cys to 1.8 for Asn. These TIMS results strongly demonstrate the powerful effect of using oligosaccharide as a selector for chiral AAs differentiation.

TIMS Separation for Chiral AA by Incorporating Both Copper Ion and Tetrasaccharide. Generally, chiral selectors are used with metal ions, especially the copper ion,[9,10,13,25−27] which is widely used in chiral analysis, to enable a larger gas-phase structure difference. Therefore, we further explored the influence of copper ions on the TIMS analysis of tetrasaccharide-AA complexes. A representative mass spectrum is shown in Figure S4. Compared to the above use of metal-free tetrasaccharide complexes for chiral Arg and Trp in Figure 4, the TIMS separation could be greatly improved by choosing the copper-bound trimeric ions [STAC + AA + Cu−H$]^+$ in Figure 5. Specifically, while Figure 4 shows that the optimum oligosaccharide complex could achieve half-valley resolution for Arg with $r \sim 0.86$ and nearly baseline separation for Trp with $r \sim 1.24$ in the TIMS dimension, Figure 5 presents nearly

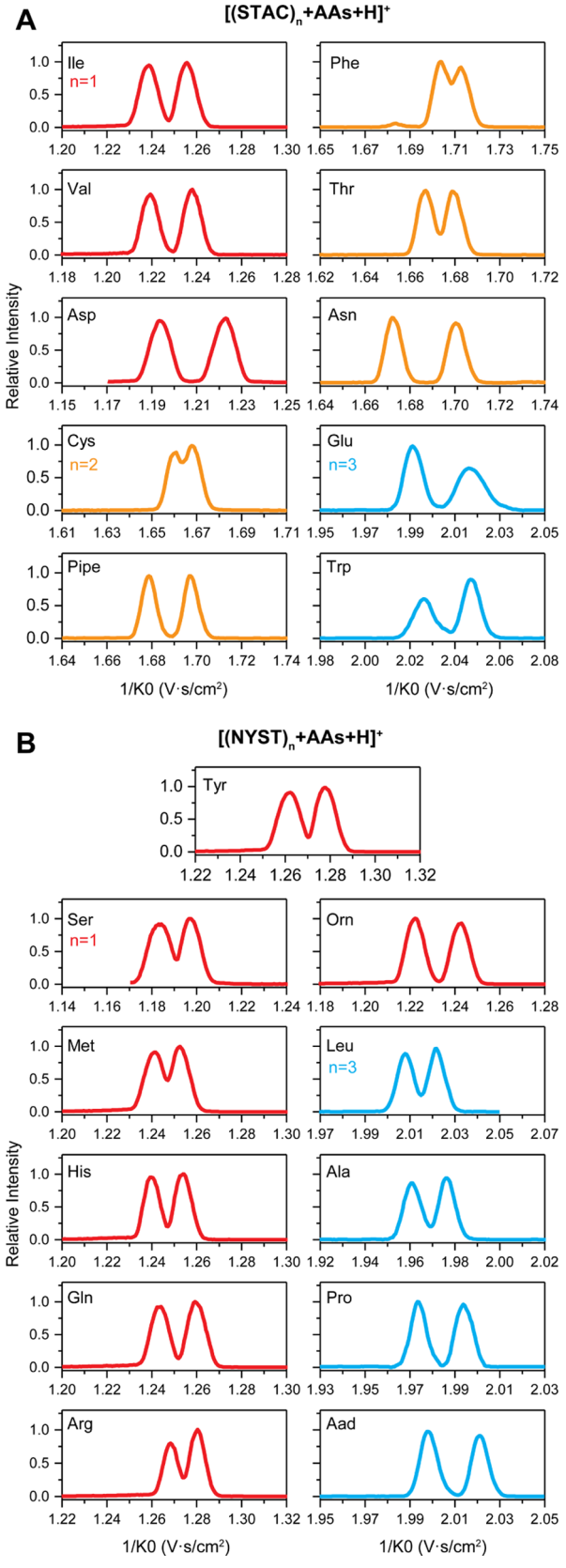

Figure 4. Optimum TIMS separation for each chiral AA mixture used in this study by choosing (A) complexes $[(STAC)_n$ + AA + H$]^+$ and (B) complexes $[(NYST)_n$ + AA + H$]^+$ (n = 1, 2, 3). The distributions of complexes [M + AA + H$]^+$, $[(M)_2$ + AA + H$]^+$, and $[(M)_3$ + AA + H$]^+$ are colored in red, yellow, and blue, respectively.

https://dx.doi.org/10.1021/acs.analchem.0c03461
Anal. Chem. 2021, 93, 859−867

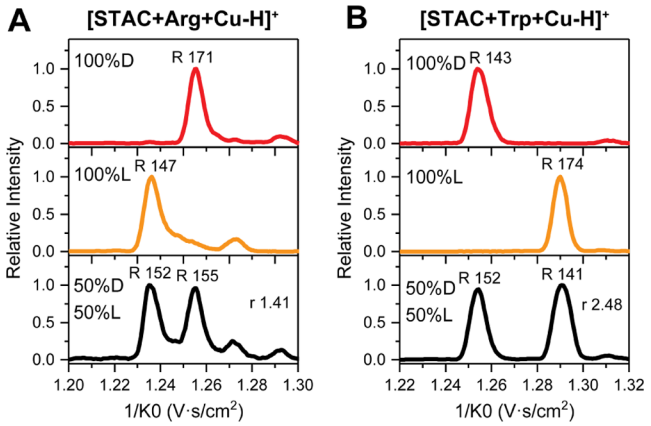

Figure 5. TIMS separation for chiral AA complexes $[STAC + AA + Cu-H]^+$, including (A) Arg and (B) Trp. The $1/K_0$ distributions of the individual samples and sample mixtures are depicted in colored and black traces, respectively. The R and r values are also given.

baseline separation ($r \sim 1.41$) and baseline separation ($r \sim 2.48$) using copper included complexes for chiral Arg and Trp, respectively. Although the presence of multiple peaks impeded the separation of the sample mixture, as much as 1.64 and 2 resolution improvement compared with the optimum metal-free complexes was experimentally observed for the copper complex ions $[STAC + Arg + Cu-H]^+$ and $[STAC + Trp + Cu-H]^+$, respectively. The minor peaks seem to come from the ions $[STAC + Arg + Cu + Cl]^+$ presumably due to the direct loss of Cl^- on the way from the TIMS analyzer to the detector.

The TIMS analysis of Cu^{2+}−tetrasaccharide complexes for all AAs was further investigated, and relevant experimental results are listed in Tables S2 and S3. It is worth noting that higher resolution for most Cu^{2+}−STAC−AA complexes was realized using trimeric ions $[STAC + AA + Cu-H]^+$ rather than tetrameric ions $[(STAC)_2 + AA + Cu-H]^+$ in Table S2, while higher differentiation ability was almost provided by choosing tetrameric ions $[(NYST)_2 + AA + Cu-H]^+$ rather than trimeric ions $[NYST + AA + Cu-H]^+$ in Table S3. Another interesting phenomenon is that nearly opposite chiral AA elution orders were presented for the Cu^{2+}−STAC−AA complexes and Cu^{2+}−NYST−AA complexes in Tables S2 and S3. The elution orders for Cu^{2+}−tetrasaccharide−AA complexes seem to be largely influenced by the number of incorporated tetrasaccharides. The binding sites of amino acids presumably differ from a single tetrasaccharide complex to a dual tetrasaccharide complex, which leads to a dramatic conformational change for Cu^{2+}−tetrasaccharide−AA complexes. The optimum resolution distributions for Cu^{2+}−STAC−AA complexes and Cu^{2+}−NYST−AA complexes are presented in Figure 6A. The resolution of the optimum metal-free tetrasaccharide complexes investigated above was displayed for comparison. For unresolved chiral AA complexes in the sample mixture, the resolution values were obtained from the TIMS analysis of individual samples. As shown in Figure 6A, although a slightly lower resolution was shown for Orn, Pipe, and Asp, other 17 pairs of Cu^{2+}−tetrasaccharide−AA complexes could achieve a higher resolution when compared to the metal-free tetrasaccharide complexes for chiral AA separation. This means that the binding of copper ions could further improve the mobility difference of chiral AA based on tetrasaccharide incorporation. For Cys, no copper-bound complex was observed because cysteine is easily oxidized to cystine under normal conditions.[34] To see the detailed resolution increment of chiral AA separation using Cu^{2+}−tetrasaccharide−AA complexes, the resolution ratios of Cu^{2+}−tetrasaccharide−AA complexes to tetrasaccharide-only complexes are plotted in Figure 6B. The Cu^{2+}−tetrasacchar-

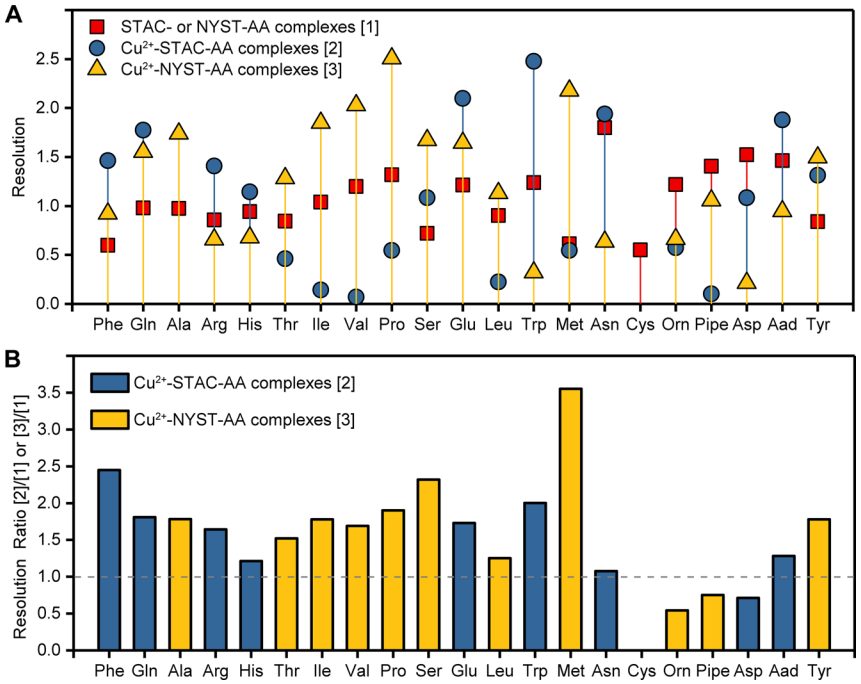

Figure 6. (A) Optimum resolution distribution for [1] protonated tetrasaccharide−AA complexes, [2] Cu^{2+}−STAC−AA complexes, and [3] Cu^{2+}−NYST−AA complexes. (B) Maximal resolution ratio of the Cu^{2+}−tetrasaccharide−AA complexes ([2] or [3]) to the protonated tetrasaccharide−AA complexes.

https://dx.doi.org/10.1021/acs.analchem.0c03461
Anal. Chem. 2021, 93, 859−867

ide−AA complexes could provide an additional 52% resolution improvement ($R \sim 1.64$) on average on top of the already achieved separation in Figure 4. Especially for Met, as much as 255% resolution improvement was experimentally observed. All of these examples fully demonstrated the powerful potential of the incorporation of both the Cu^{2+} ion and tetrasaccharide on chiral AA differentiation even on the basis that the metal-free method has already resolved all chiral AAs in this study.

CONCLUSIONS

The great potential of oligosaccharides as selectors for rapid chiral AA separation on TIMS-MS has been demonstrated through this study. Using high resolving power IMS, the separation of 21 amino acids, including small molecules (e.g., Ala and Cys), could be achieved by incorporating nonreducing tetrasaccharides without using metal ions, and the identification can be accomplished through simply mixing the analyte and tetrasaccharide solutions followed by direct infusion TIMS-MS analysis. By incorporating both the copper ion and tetrasaccharide, as much as a 52% resolution improvement could be further achieved in comparison to only using nonreducing tetrasaccharides. This method is particularly suitable for the relatively low resolving power commercial IMS instrument due to a significantly increased mobility difference between enantiomeric complexes. Another benefit is that more oligosaccharides are available in addition to the tetrasaccharides used in this study, which may make the oligosaccharide incorporation strategy a new area to explore for routine IMS-based chiral analysis.

ASSOCIATED CONTENT

Supporting Information

The Supporting Information is available free of charge at https://pubs.acs.org/doi/10.1021/acs.analchem.0c03461.

Mass spectra of tetrasaccharide and AA mixtures (Figure S1); TIMS separation for the protonated AAs and tetrasaccharide−AA complexes (Figure S2); $1/K_0$ vs m/z 2D scatter plots for all tetrasaccharide−AA complexes (Figure S3); mass spectrum of a tetrasaccharide, AA, and $CuCl_2$ mixture (Figure S4); and tables of separation parameters (Tables S1−S3) (PDF)

AUTHOR INFORMATION

Corresponding Authors

Jiancheng Yu − *Institute of Mass Spectrometry and Faculty of Electrical Engineering and Computer Science, Ningbo University, Ningbo 315211, P. R. China*; Email: yujiancheng@nbu.edu.cn

Keqi Tang − *Institute of Mass Spectrometry and School of Material Science and Chemical Engineering, Ningbo University, Ningbo 315211, P. R. China*; Email: tangkeqi@nbu.edu.cn

Authors

Chengyi Xie − *Institute of Mass Spectrometry and Faculty of Electrical Engineering and Computer Science, Ningbo University, Ningbo 315211, P. R. China*; orcid.org/0000-0003-2831-0695

Liancheng Gu − *Department of Chemistry, Fudan University, Shanghai 200438, P. R. China*

Qidi Wu − *Institute of Mass Spectrometry and Faculty of Electrical Engineering and Computer Science, Ningbo University, Ningbo 315211, P. R. China*

Lei Li − *Institute of Mass Spectrometry and School of Material Science and Chemical Engineering, Ningbo University, Ningbo 315211, P. R. China*; orcid.org/0000-0002-4269-7745

Chenlu Wang − *Institute of Mass Spectrometry and School of Material Science and Chemical Engineering, Ningbo University, Ningbo 315211, P. R. China*

Complete contact information is available at: https://pubs.acs.org/10.1021/acs.analchem.0c03461

Notes

The authors declare no competing financial interest.

ACKNOWLEDGMENTS

This work was supported by the National Natural Science Foundation of China (Grant No. 61971248), National Key Research and Development Program of China (Grant No. 2017YFC1001700), Key Research and Development Program of Zhejiang Province (Grant No. 2020C03064), Science and Technology Major Project of Ningbo (Grant No. 2018B10075), and the Special Research Funding from the Marine Biotechnology and Marine Engineering Discipline Group in Ningbo University (Grant No. 422004582) and sponsored by the K.C. Wong Magna Fund in Ningbo University.

REFERENCES

(1) Bentley, R. *Chem. Soc. Rev.* **2005**, *34*, 609−624.
(2) Wnendt, S.; Zwingenberger, K. *Nature* **1997**, *385*, 303−304.
(3) Schurig, V. *TrAC, Trends Anal. Chem.* **2002**, *21*, 647−661.
(4) Ilisz, I.; Aranyi, A.; Pataj, Z.; Péter, A. *J. Pharm. Biomed. Anal.* **2012**, *69*, 28−41.
(5) Kalíková, K.; Šlechtová, T.; Vozka, J.; Tesařová, E. *Anal. Chim. Acta* **2014**, *821*, 1−33.
(6) Van Eeckhaut, A.; Michotte, Y. *Electrophoresis* **2006**, *27*, 2880−2895.
(7) Cheng, Y.; Hercules, D. M. *J. Mass Spectrom.* **2001**, *36*, 834−836.
(8) Seymour, J. L.; Tureček, F.; Malkov, A. V.; Kočovský, P. *J. Mass Spectrom.* **2004**, *39*, 1044−1052.
(9) Tao, W. A.; Wu, L.; Cooks, R. G. *Chem. Commun.* **2000**, *20*, 2023−2024.
(10) Tao, W. A.; Clark, R. L.; Cooks, R. G. *Anal. Chem.* **2002**, *74*, 3783−3789.
(11) Yao, Z. P.; Wan, T. S. M.; Kwong, K. P.; Che, C. T.; et al. *Chem. Commun.* **1999**, *20*, 2119−2120.
(12) Yao, Z. P.; Wan, T. S. M.; Kwong, K. P.; Che, C. T. *Anal. Chem.* **2000**, *72*, 5383−5393.
(13) Huang, L.; Gao, Z.; Yin, X.; He, Q.; Pan, Y. *Rapid Commun. Mass Spectrom.* **2020**, *34*, No. e8764.
(14) Ramirez, J.; Ahn, S.; Grigorean, G.; Lebrilla, C. B. *J. Am. Chem. Soc.* **2000**, *122*, 6884−6890.
(15) Botta, B.; Botta, M.; Filippi, A.; Tafi, A.; Monache, G. D.; Speranza, M. *J. Am. Chem. Soc.* **2002**, *124*, 7658−7659.
(16) Bagheri, H.; Chen, H.; Cooks, R. G. *Chem. Commun.* **2004**, *23*, 2740−2741.
(17) Wu, Q.; Wang, J. Y.; Han, D. Q.; Yao, Z. P. *TrAC, Trends Anal. Chem.* **2020**, *124*, No. 115801.
(18) May, J. C.; Goodwin, C. R.; Lareau, N. M.; Leaptrot, K. L.; Morris, C. B.; Kurulugama, R. T.; Mordehai, A.; Klein, C.; Barry, W.; Darland, E.; Overney, G.; Imatani, K.; Stafford, G. C.; Fjeldsted, J. C.; McLean, J. A. *Anal. Chem.* **2014**, *86*, 2107−2116.

(19) Giles, K.; Pringle, S. D.; Worthington, K. R.; Little, D.; Wildgoose, J. L.; Bateman, R. H. *Rapid Commun. Mass Spectrom.* **2004**, *18*, 2401−2414.
(20) Fernandez-Lima, F.; Kaplan, D. A.; Suetering, J.; Park, M. A. *Int. J. Ion Mobility Spectrom.* **2011**, *14*, 93−98.
(21) Reischl, G. P. *Aerosol Sci. Technol.* **1991**, *14*, 5−24.
(22) Shvartsburg, A. A.; Li, F.; Tang, K.; Smith, R. D. *Anal. Chem.* **2006**, *78*, 3706−3714.
(23) Han, D. Q.; Yao, Z. P. *TrAC, Trends Anal. Chem.* **2020**, *123*, No. 115763.
(24) Dwivedi, P.; Wu, C.; Matz, L. M.; Clowers, B. H.; Siems, W. F.; Hill, H. H. *Anal. Chem.* **2006**, *78*, 8200−8206.
(25) Domalain, V.; Hubert-Roux, M.; Tognetti, V.; Joubert, L.; Lange, C. M.; Rouden, J.; Afonso, C. *Chem. Sci.* **2014**, *5*, 3234−3239.
(26) Yu, X.; Yao, Z. P. *Anal. Chim. Acta* **2017**, *981*, 62−70.
(27) Mie, A.; Jörntén-Karlsson, M.; Axelsson, B. O.; Ray, A.; Reimann, C. T. *Anal. Chem.* **2007**, *79*, 2850−2858.
(28) Zhang, J. D.; Kabir, K. M. M.; Donald, W. A. *Anal. Chim. Acta* **2018**, *1036*, 172−178.
(29) Zhang, J. D.; Kabir, K. M. M.; Lee, H. E.; Donald, W. A. *Int. J. Mass Spectrom.* **2018**, *428*, 1−7.
(30) Pérez-Míguez, R.; Bruyneel, B.; Castro-Puyana, M.; Marina, M. L.; Somsen, G. W.; Dominguez-Vega, E. *Anal. Chem.* **2019**, *91*, 3277−3285.
(31) Giles, K.; Ujma, J.; Wildgoose, J.; Pringle, S.; Richardson, K.; Langridge, D.; Green, M. *Anal. Chem.* **2019**, *91*, 8564−8573.
(32) Ujma, J.; Ropartz, D.; Giles, K.; Richardson, K.; Langridge, D.; Wildgoose, J.; Green, M.; Pringle, S. *J. Am. Soc. Mass Spectrom.* **2019**, *30*, 1028−1037.
(33) Michelmann, K.; Silveira, J. A.; Ridgeway, M. E.; Park, M. A. *J. Am. Soc. Mass Spectrom.* **2015**, *26*, 14−24.
(34) Gatlin, C. L.; Turecek, F.; Vaisar, T. *J. Am. Chem. Soc.* **1995**, *117*, 3637−3638.

https://dx.doi.org/10.1021/acs.analchem.0c03461
Anal. Chem. 2021, 93, 859−867